THE JOURNAL OF PHYSICAL CHEMISTRY A
A JOURNAL OF THE AMERICAN CHEMICAL SOCIETY

pubs.acs.org/JPCA

Article

Kinetics of the Simplest Criegee Intermediate CH_2OO Reaction with *tert*-Butylamine

Yang Chen, Haotian Jiang, Siyue Liu, Jiayu Shi, Yuqi Jin, Xueming Yang, and Wenrui Dong*

Cite This: *J. Phys. Chem. A* 2023, 127, 2432−2439

Read Online

ACCESS | Metrics & More | Article Recommendations | Supporting Information

ABSTRACT: The kinetics of the simplest Criegee intermediate (CH_2OO) reaction with *tert*-butylamine ($(CH_3)_3CNH_2$) was studied under pseudo-first-order conditions with the OH laser-induced fluorescence (LIF) method at the temperature range of 283−318 K and the pressure range of 5−75 Torr. Our pressure-dependent measurement showed that at 5 Torr—the lowest pressure measured in the current experiment—this reaction was under the high-pressure limit condition. At 298 K, the reaction rate coefficient was measured to be $(4.95 \pm 0.64) \times 10^{-12}$ cm^3 molecule^{-1} s^{-1}. The title reaction was observed to be negative temperature-dependent; the activation energy of (-2.82 ± 0.37) kcal mol^{-1} and the pre-exponential factor of $(4.21 \pm 0.55) \times 10^{-14}$ cm^3 molecule^{-1} s^{-1} were derived from the Arrhenius equation. The rate coefficient of the title reaction is slightly larger than $(4.3 \pm 0.5) \times 10^{-12}$ cm^3 molecule^{-1} s^{-1} of the CH_2OO reaction with methylamine; the electron inductive effect and the steric hindrance effect might play a role in contributing to such difference.

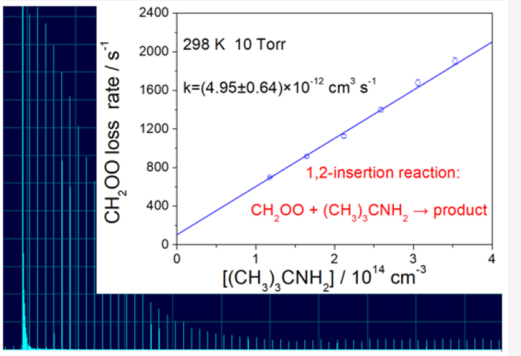

1. INTRODUCTION

Reactive zwitterionic Criegee intermediates could be generated from the ozonolysis of alkenes.[1] Ozone adds across the C=C double bond of alkenes, forming a five-member ring primary ozonide (POZ), which promptly decomposes to carbonyl oxide, namely Criegee intermediate (CI). This reaction is exothermic by about 48−60 kcal mol^{-1}.[2] Hence, some CIs are vibrationally excited (denoted as CIs*). The newly formed CIs* could isomerize; or decompose to species such as OH, HO_2, and organic radicals; or are thermalized by the bath gas, forming the stabilized Criegee intermediate (denoted as SCIs).[3] SCIs could decompose to OH radicals,[4] as CIs* do. The contribution of alkene ozonolysis to the atmospheric OH concentration differs markedly, depending on factors such as region and climate. For example, according to the field measurements, alkene ozonolysis is responsible for more than half of OH production in summer and over 90% in winter in the west Midlands, UK;[5,6] 24% in summer in the urban area of Santiago, Chile;[7] and 29% in summer and up to 43% during the heat wave period in a site northeast of London.[5] Alkene ozonolysis accounts for almost all OH production at night.[5,8] Therefore, the decomposition of SCIs is a considerable source of OH—especially in winter or at night when H_2O reaction with $O(^1D)$ is constrained by either the low concentration of H_2O or the lack of Ultra Violet (UV) light that photolyze O_3 to form $O(^1D)$.[9−11] Moreover, SCIs could be consumed by trace atmospheric species, e.g., H_2O, NO_2, SO_2, alcohols, and carboxylic acids,[12−17] either because of the high reactivity, such as that between SCIs and carboxylic acids, or because of the high concentration of the coreactant such as H_2O. Considering the steady-state concentration of SCIs ($10^3 \sim 10^6$ cm^{-3}) in the atmosphere,[18,19] the reactions between SCIs and these species are nontrivial in the atmospheric conditions. They should be considered in atmospheric chemistry models.

Amines are an important class of organic compounds in the atmosphere, which are emitted from various sources, including chemical manufacturing, animal husbandry, ocean, biomass burning, and tobacco smoke.[20−22] The typical concentration of amines is 14−23% of that of ammonia,[23] whose mixing ratio over continents is between 0.1 and 10 ppb,[24] and this value could reach a few ppm near areas of extensive livestock operations.[25] Some atmospheric reactions of amines, such as with acids (HCl, HNO_3, H_2SO_4, and organic acids)[26,27] and atmospheric oxidants (O_3, NO_x)[26] were reported. However, the study on the reactions of amines with SCI is scarce, and this reaction might contribute to the deposition of the atmospheric amines and the formation of secondary organic aerosol (SOA).

The most abundant atmospheric amines are low-molecular-weight aliphatic amines with one to six carbon atoms.[20] Methylamine is the simplest amine, which reacts with CH_2OO via the 1,2-insertion mechanism.[28,29] There were two results on

Received: November 8, 2022
Revised: February 20, 2023
Published: March 13, 2023

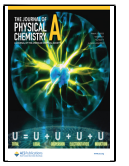

https://doi.org/10.1021/acs.jpca.2c07854
J. Phys. Chem. A 2023, 127, 2432−2439

the rate coefficient measurement—$(4.3 \pm 0.5) \times 10^{-12}$ cm^3 molecule^{-1} s^{-1} from multiplexed photoionization mass spectrometry (MPIMS) at 298 K and 4 Torr (He as bath gas),[28] and $(4.41 \pm 0.7) \times 10^{-12}$ cm^3 molecule^{-1} s^{-1} (ESI of ref 28) from cavity ring-down spectroscopy (CARDS) at 298 K and 10 Torr (N_2 as bath gas), respectively. The reaction product, 1-hydroperoxy- *N*-methylmethanamine, a functionalized organic hydroperoxide detected by MPIMS, could contribute to the formation of atmospheric SOA. *tert*-Butylamine, with each H atom on the methyl group of methylamine substituted by methyl, is emitted to the atmosphere mainly from the rubber industry.[20] For example, high-performance liquid chromatography with mass spectrometric detection was used to analyze air samples from a tire repair shop, and *tert*-butylamine of 0.3 μg m^{-3} was detected.[22] The data on the *tert*-butylamine concentration in the atmosphere is absent, while its concentration should be higher in areas such as that dense with rubber industry. From the study of CH_2OO reaction with *tert*-butylamine, in combination with the previous results of CH_2OO reaction with methylamine, we may draw some general conclusions about Criegee intermediates reactions with amines.

In the current work, the OH laser-induced fluorescence method was applied to measure the rate coefficients of CH_2OO reaction with *tert*-butylamine at temperatures ranging from 283 to 318 K and pressures from 5 to 75 Torr. The rate coefficient was compared with that of the CH_2OO reaction with methylamine, and the origin of the difference in the rate coefficient between the two reactions was discussed. Finally, the atmospheric effect of the title reaction was discussed.

2. EXPERIMENTAL SECTION

The apparatus for the laser-induced fluorescence was described in detail in our previous work,[30−32] and a brief description is introduced here. Ar flowed over liquid CH_2I_2 (stabilized at 35 °C) in a glass bubbler that was kept in a water bath. Buffer gas Ar (99.999%), O_2 (99.995%), $(CH_3)_3CNH_2$ (3% seeded in Ar), and CH_2I_2 (Alfa Aeser, > 99%) flowed continuously through a premixed manifold to a 75 cm-long quartz flow tube reactor. The flow rate of these gases was controlled by a series of calibrated mass flow controllers (MKS, GM50A Series). A capacitance manometer (MKS Baratron) and an exhaust throttle valve (MKS, 653B) were utilized to control the pressure of the flow reactor actively. The UV absorption of CH_2I_2 was measured with a deep UV LED (DUV325-H46, Roithner Lasertechnik, wavelength centered at 322.4 nm with full-width half-maximum of 11 nm) and an amplified photodetector (PDB450A, Thorlabs). The concentration of CH_2I_2 was then deduced from the known absorption cross-section[33] and the LED emission profile that was measured with a spectrometer (Seeman, S3000−UV−NIR). The typical concentration of CH_2I_2 was ca. 1.5×10^{14} molecules cm^{-3}.

A 248 nm pulsed excimer laser (Coherent, COMPexPro 50), with a typical laser fluence of 17 mJ cm^{-2}, was used to photolyze CH_2I_2 in the presence of O_2. The probe laser (2 mm diameter, 40 nJ) was generated by frequency doubling of a dye laser (Rhodamine 590 dye) which was pumped by the second harmonic of a Nd: YAG laser (Edgewave INNOSLAB: IS12II-ET, 10 kHz). The probe wavelength, 282 nm, corresponds to the $P_1(1)$ line of the (1,0) band of the OH ($A^2\sum^+ \leftarrow X^2\prod$) transition. The time delay between the photolysis and probe radiation was controlled by a delay generator (Stanford Research System, DG645). The two beams intersected at a right angle in the 75 cm-long quartz reaction cell. The OH fluorescence that is emitted in the direction perpendicular to both the photolysis and the probe beam will pass through a quartz lens and a stack of filters (Schott UG11, Semrock FF02−320/40−25, Semrock FF01−315/15−25) before it was amplified by a photomultiplier tube (PMT, Electron PDM9111-CP-TTL). The signal from the PMT was fed to a multichannel scaler (Ortec, EASY-MCS) and recorded on a computer. Typically, a decay profile was obtained by accumulating signals from 1500 photolysis laser pulses to increase the signal-to-noise ratio.

3. RESULTS AND DISCUSSION

3.1. Kinetic Model and the OH Decay Profiles. The rate coefficient for the reaction of CH_2I with O_2 was reported to be 1.39×10^{-12} cm^3 molecule^{-1} s^{-1}.[34] The typical concentration of O_2 in the current experiment is 1.5×10^{16} cm^{-3}; hence, CH_2OO was formed within tens of microseconds. In comparison, the consumption of CH_2OO under the present experimental condition took several milliseconds. Therefore, the kinetics of the formation of CH_2OO was not included in the following kinetic model.

CH_2OO from the CH_2I+O_2 reaction may not be thermalized, and some might be highly vibrationally excited (CH_2OO^*), as was proposed by Stone et al.[35] The CH_2OO^*, if being produced, could either be thermalized within hundreds of nanoseconds at 298 K and 10 Torr—considering the average energy transfer per collision $\langle E_{down} \rangle$ of 32.6−123 cm^{-1}[35,36] —or decompose. Therefore, the decay profiles in Figure 1 represent the kinetics of the thermalized CH_2OO.

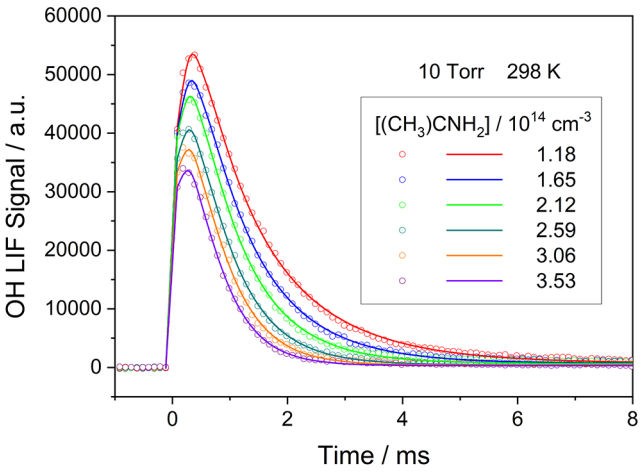

Figure 1. OH time-dependent profiles in the presence of various concentrations of *tert*-butylamine.

Some thermalized CH_2OO could also distribute in the low vibrationally excited states. Huang et al. attributed several infrared absorption bands to vibrationally excited states of CH_2OO (at 15 Torr and 343 K in a flow tube reactor), due to the better agreement between their experimental results and simulated spectrum based on excited-state rotational parameters.[37] With the electric discharge of gas mixture (CH_2I_2, O_2, and Ne) in a molecular beam, a method to generate CH_2OO different from ours of 248 nm laser photolysis in a flow tube reactor, Nakajima et al. observed the vibrationally excited CH_2OO in their microwave spectra.[38]

https://doi.org/10.1021/acs.jpca.2c07854
J. Phys. Chem. A 2023, 127, 2432−2439

Regarding the OH product vibrational states distribution, both OH (v″ = 0) and OH (v″ = 1) were observed upon excitation of OH through the $A^2\sum^+$ (v′ = 1) ←$X^2\prod$ (v″ = 0)/ $A^2\sum^+$ (v′ = 2) ←$X^2\prod$ (v″ = 1) transition by 282/288 nm radiation.[35,39] The origin of near-instant OH (v″ = 0) and OH (v″ = 1) could be attributed to the reaction of excited CH_2I^*[40] with O_2 and/or the rapid decomposition of excited CH_2OO^*.[35,40] OH in higher vibrational levels (v″ ≥ 2), if it exists, should have the same origin as OH (v″ = 1) and will undergo collisional relaxation to OH (v″ = 1) rapidly.[35] In the current experiment, the first probe laser pulse was fired about 80 μs later than the photolysis laser pulse, which was long enough for sufficient relaxation of OH (v″ ≥ 2).

The time evolution of OH (v″ = 0) concentration, as shown in Figure 1, was the result of the production of OH (v″ = 0) from decomposition of thermalized CH_2OO—with reported rates varying from 0.001 to 0.26 s^{-1},[35,36,41] the relaxation of near-instant produced OH (v″ = 1), and the consumption of OH (v″ = 0) by species such as CH_2I_2. Analysis has shown that the difference between the rate coefficients, derived from fitting time-dependent profiles of OH (v″ = 0) with and without considering the relaxation of OH (v″ = 1) to OH (v″ = 0), is less than 4% at 10 Torr and less than 1% at 50 Torr.[39] In the current work, the time-dependent profiles of OH (v″ = 0) were fitted with Equation 1, which does not contain the relaxation of OH (v″ = 1), and the error caused by this was included in the error analysis (see the ESI).

Upon generation, the thermalized CH_2OO is consumed through the following reactions.

$$CH_2OO \rightarrow OH + HCO \qquad k_{1a} \qquad \text{(R1a)}$$

$$\rightarrow \text{other products} \qquad k_{1b} \qquad \text{(R1b)}$$

$$\rightarrow \text{physical losses} \qquad k_{1c} \qquad \text{(R1c)}$$

$$CH_2OO + CH_2OO \rightarrow \text{products} \qquad k_2 \qquad \text{(R2)}$$

$$CH_2OO + (CH_3)_3CNH_2 \rightarrow \text{products} \qquad k_3 \qquad \text{(R3)}$$

$$CH_2OO + X \rightarrow \text{products} \qquad k_4 \qquad \text{(R4)}$$

The consumption of OH radicals could be summarized by reaction (R5).

$$OH + Y \rightarrow \text{products} \qquad k_5 \qquad \text{(R5)}$$

In addition to reacting with *tert*-butylamine, CH_2OO is also consumed by its unimolecular dissociation (R1a and R1b); physical losses (R1c)—mainly from wall loss and the diffusion out of the detection area; self-reaction (R2); and bimolecular reactions with other species denoted as X, including I, IO, and CH_2I_2. OH is consumed by species denoted as Y, including IO and CH_2I_2.

As $[(CH_3)_3CNH_2]$ (ca. 1.2−3.5 × 10^{14} molecules cm^{-3}) is significantly greater than $[CH_2OO]$, the reaction of CH_2OO with *tert*-butylamine is under pseudo-first-order approximation conditions. Integrating relevant rate equations, together with applying steady-state approximation to OH, the time-dependent OH (v″ = 0, N″ = 1) profile, $S_{OH}(t)$, could be described by the following equation (see our previous work for more details).[39,42,43]

$$S_{OH}(t) = \frac{A_0(k_1 + k_3' + k_4')}{(k_1 + k_3' + k_4')e^{(k_1+k_3'+k_4')t} + 2k_2[CH_2OO]_0[e^{(k_1+k_3'+k_4')t} - 1]} - A_1 e^{-k_5' t} \qquad (1)$$

where

$$A_0 = \gamma \frac{k_{1a}[CH_2OO]_0}{k_5' - (k_1 + k_3' + k_4')}$$

$$A_1 = \gamma\left(\frac{k_{1a}[CH_2OO]_0}{k_5' - (k_1 + k_3' + k_4')} - [OH]_0\right)$$

In eq 1, $k_3' = k_3[(CH_3)_3CNH_2]$, $k_4' = k_4[X]$, and $k_5' = k_5[Y]$. $[OH]_0$ denotes the OH concentration from the decomposition of excited CH_2OO, and $[CH_2OO]_0$ is the initial CH_2OO concentration. γ is the detection efficiency of OH. During the fitting of OH signals, A_0, A_1, $k_1 + k_3' + k_4'$ and k_5' were local parameters, while k_2 was a global parameter and was fixed at 8 × 10^{-11} cm^3 $molecule^{-1}$ s^{-1}.[44] $[CH_2OO]_0$ was fixed to the value calculated according to the known $[CH_2I_2]$, fluence of the photolysis radiation, and the yield of CH_2OO.

Plotting $k_1 + k_3' + k_4'$ against the concentration of *tert*-butylamine at a given temperature and pressure, the slope and the intercept of the linear fit represent k_3 and $k_1 + k_4'$, respectively. Note that reactions R1, R4, R5, and the yield of OH, even if they are temperature or pressure-dependent, could only alter the values of A_0 and A_1 instead of affecting the accuracy of k_3.

Figure 1 shows the selected time-dependent profiles of the OH signals at 10 Torr and 298 K. Solid lines are the fit of experimental data (empty circles) with eq 1 by using First Optimization software (1stOpt 7.0, 7D-soft High Technology Inc.). Note that, since $k_5' > k_1 + k_3' + k_4'$ under the current experimental conditions (See Table S1.), the rise of the OH profile represents OH loss kinetics, and the decay of the OH profile represents OH formation kinetics that originated from the decomposition of CH_2OO. Therefore, the decay of the OH profile represents the consumption of CH_2OO. Figure 1 shows that the higher the *tert*-butylamine concentration was, the faster CH_2OO was consumed, indicating the reaction of CH_2OO with *tert*-butylamine.

3.2. Temperature-Dependent Rate Coefficients. The plots of effective pseudo-first-order loss rate k_3' against $[(CH_3)_3CNH_2]$ at 10 Torr and four different temperatures ranging from 283 to 318 K are shown in Figure 2. The fitting parameters of the time-dependent OH profiles at four temperatures are listed in Table S1. Our result shows that k_3 is not sensitive to $[CH_2OO]_0$, indicating the consumption of CH_2OO was dominated by bimolecular reactions instead of its self-reaction (for details, see Table S2 of ESI). At each temperature, the error bar of k_3' represents 1σ uncertainty of the fit of the OH time-dependent profile, and the linear relationship between k_3' and $[(CH_3)_3CNH_2]$ is shown by a solid line. The rate coefficients were measured to be (6.40 ± 0.83), (4.95 ± 0.64), (4.23 ± 0.55), (3.69 ± 0.48) × 10^{-12} cm^3 $molecule^{-1}$ s^{-1} at 283, 298, 308, and 318 K after averaging the results from five sets of experimental data at the same temperature (for details, see Table S4). The title reaction exhibits apparent negative temperature dependence, which is consistent with the reaction of CH_2OO with NH_3 and CH_3NH_2, as well as with some other bimolecular reactions of CH_2OO that proceed through 1, 2-insertion.[28,31,45,46]

https://doi.org/10.1021/acs.jpca.2c07854
J. Phys. Chem. A 2023, 127, 2432−2439

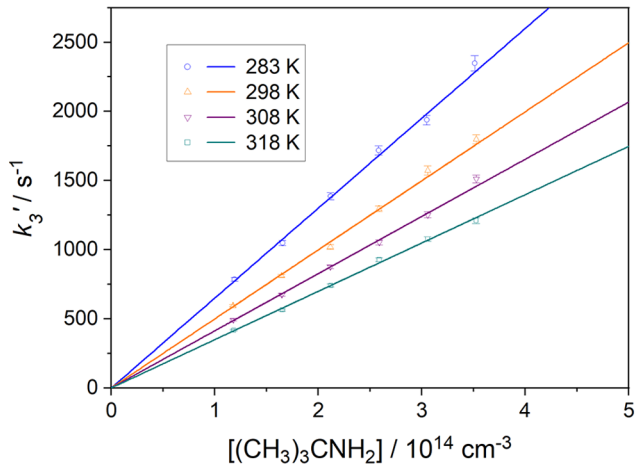

Figure 2. Fitted values of k_3' plotted against the concentration of *tert*-butylamine. The slopes of each straight line give the rate coefficients of CH_2OO reaction with *tert*-butylamine at the corresponding temperature.

The Arrhenius plot of the bimolecular rate coefficients for the reaction of CH_2OO with $(CH_3)_3CNH_2$ at 10 Torr is shown in Figure 3. Open circles are experimental data, and the

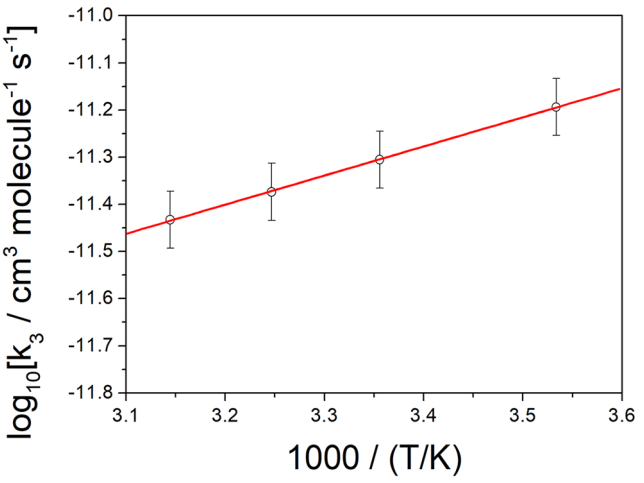

Figure 3. Arrhenius plot of the bimolecular rate coefficients for CH_2OO + $(CH_3)_3CNH_2$ reaction at 10 Torr. The error bar is 13% of each rate coefficient.

red line is the fit of k_3 with the Arrhenius equation, $k(T) = A\exp(-E_a/RT)$. The experimental error was estimated to be about 13% (see the ESI). Considering this, the activation energy of (-2.82 ± 0.37) kcal mol^{-1} and the pre-exponential factor of $(4.21 \pm 0.55) \times 10^{-14}$ cm^3 molecule^{-1} s^{-1} were determined.

3.3. Pressure-Dependent Rate Coefficient. The rate coefficients of the title reaction at pressures ranging from 5 to 75 Torr and 298 K are shown in Figure 4. Rate coefficients at pressures higher than 75 Torr were not measured, as the collisional quenching of OH ($A^2\sum^+$) was significant. Figure 4 exhibits no noticeable pressure dependence, indicating that the title reaction was under the high-pressure limit condition at a pressure as low as 5 Torr.

The reaction of CH_2OO with *tert*-butylamine should proceed through the 1,2-insertion of CH_2OO into the N−H bond of *tert*-butylamine, similar to the reaction of CH_2OO

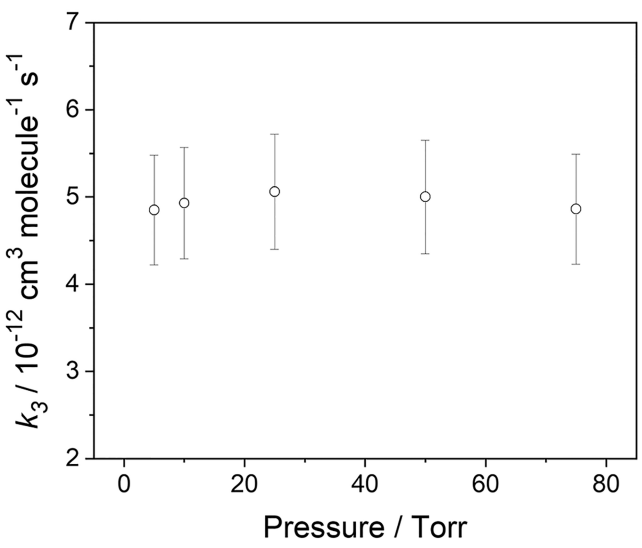

Figure 4. Measured rate coefficients of the title reaction as a function of total pressure at 298 K. The plotted error bar is 13% of each rate coefficient.

with methylamine.[28] Such a reaction mechanism is typical for bimolecular SCIs reactions in which the coreactants contain covalent bonds with hydrogen.[29] A representative energy profile that describes the reaction pathway involving a five-ring transition state is shown in Figure S1.

Chhantyal-Pun et al. showed that, in terms of bimolecular reactions of CH_2OO, the rate coefficient for the 1,2-insertion reaction correlates with the labile hydrogen bond dissociation energy (BDE) of the coreactant.[29] The 1,2-insertion process gets harder as BDE increases. The rate coefficients of CH_2OO reacting with H_2O, NH_3, CH_3NH_2, CH_3OH, C_2H_5OH, $(CH_3)_2CHOH$, and $(CH_3)_3CNH_2$ as a function of BDE were plotted in Figure 5. The red line is the linear fit of the data (excluded $(CH_3)_3CNH_2$). Original data of BDE and rate coefficients are summarized in Table S6. Figure 5 shows that the rate coefficient of CH_2OO reaction with *tert*-butylamine is

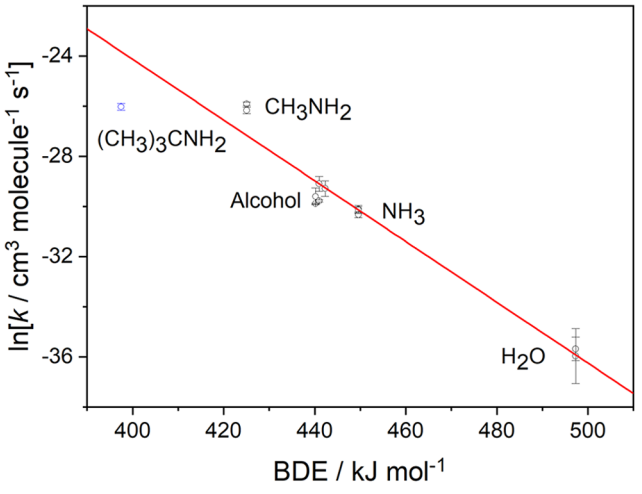

Figure 5. Rate coefficients for several 1,2-insertion reactions of CH_2OO as a function of BDE. The blue point is our experimental value. CH_3OH, C_2H_5OH, and $(CH_3)_2CHOH$ were collectively labeled as alcohol.

https://doi.org/10.1021/acs.jpca.2c07854
J. Phys. Chem. A 2023, 127, 2432−2439

Table 1. Predicted Sub-Cooled Liquid Vapor Pressures at 298 K (in Torr) for the Adduct Products of Several CH_2OO Reactions through 1,2-Insertion

coreactant	H_2O	NH_3	CH_3NH_2	HCl	CH_3OH	C_2H_5OH	$(CH_3)_3CNH_2$
/ Torr	0.05	0.24	0.70	3.80	5.17	2.80	0.21

Table 2. Predicted Partitioning Coefficients in $m^3\ \mu g^{-1}$ for the Adduct Products of Several CH_2OO Reactions through 1,2-Insertion

coreactant	H_2O	NH_3	CH_3NH_2	HCl	CH_3OH	C_2H_5OH	$(CH_3)_3CNH_2$
/ $m^3\ \mu g^{-1}$	5.81×10^{-6}	1.23×10^{-6}	3.45×10^{-7}	5.93×10^{-8}	4.61×10^{-8}	7.22×10^{-8}	7.44×10^{-7}

similar to that with methylamine, which is smaller than expected from the linear fit result.

The counterbalance of two factors might contribute to this result. First, the electron-donating inductive effect of *tert*-butyl is stronger than that of methyl, making the polar interaction between N−H in the amino group more significant, which means the hydrogen atom is more prone to dissociation. The inductive effect can also result in a stronger bond between the nitrogen and carbon atoms, making the transition state more stable. The stronger inductive effect and thus lower BDE (397.5 kJ mol^{-1} vs. 425.1 kJ mol^{-1}[147]) of *tert*-butylamine than methylamine indicate that the reaction of CH_2OO with the former should be faster than the latter. Second, the reaction of CH_2OO with *tert*-butylamine has a larger steric hindrance than that with methylamine. Excessive steric hindrance generally results in high energy and low stability for the transition state, which will decompose into reactants along reaction coordinates. The larger steric hindrance of *tert*-butylamine than that of methylamine indicates that, contrary to the electron inductive effect on these two reactions, the reaction of CH_2OO with the former should be slower than the latter. The steric hindrance effect also exists in some 1,2-insertion reactions of other SCIs. For example, the 1,2-insertion reaction of water monomer with *syn*-CH_3CHOO is substantially slower than that with *anti*-CH_3CHOO; the former was calculated to be 1.98×10^{-19}[48] and measured to be slower than 2×10^{-16} cm^3 $molecule^{-1}$ s^{-1},[49] while the latter was calculated to be 3.40×10^{-14}[48] and measured to be $(1.0-2.4) \times 10^{-14}$ cm^3 $molecule^{-1}$ s^{-1}.[48,50,51] For the reactions of ammonia with *syn*/*anti*-CH_3CHOO, the rate coefficients were calculated to be 2.70×10^{-18} and 2.73×10^{-14} cm^3 $molecule^{-1}$ s^{-1},[52] respectively, and a substantial difference in the reaction rates was also observed experimentally.[53]

4. ATMOSPHERIC EFFECT

The UV absorption cross-section of *tert*-butylamine is absent; if assuming it is similar to that of methylamine, the consumption of *tert*-butylamine from solar radiation photolysis should be weak.[54] The OH radical will play a more significant role than CH_2OO in the consumption of *tert*-butylamine, since the rate coefficient of the former reaction is larger (8.4×10^{-12} cm^3 $molecule^{-1}$ s^{-1} at 305 K and 1015 ± 1 hPa),[55] and OH ($\sim 1 \times 10^6$ cm^{-3}) is more abundant than SCIs ($10^3 \sim 10^6$ cm^{-3})[18,19] in the atmosphere. In this comparison, we assume that all the SCIs react with *tert*-butylamine at the same rate as CH_2OO does. This might overestimate the sink of *tert*-butylamine from reaction with SCIs, considering that the 1,2-insertion reactions of *syn*-CH_3CHOO—for example, with water and ammonia—are normally several orders slower than that of CH_2OO.[48,50−52] However, the title reaction may play a role under conditions where OH is scarce, such as winter or night-time. Regarding the sink of SCIs, the title reaction is negligible since SCIs are mainly consumed by their unimolecular reactions and reactions with water and water dimmer.[11,12,32,48,56−58]

Regarding the reaction product, the reaction of CH_2OO with *tert*-butylamine could directly generate functionalized organic hydroperoxide—similar to the 1,2-insertion reactions of SCIs with NH_3,[28,52] H_2O,[41,48,56] H_2S,[59,60] and CH_3OH[16,45,61−63] —which have larger molecular weights and lower vapor pressures, and thus more likely to partition into an organic aerosol to form SOA. For organic compounds that are solids at room temperature and pressure but could exist as components of subcooled liquid aerosol,[64,65] subcooled liquid vapor pressure and partition coefficient are widely used to predict their gas-particle partitioning behavior. Vapor pressures of several 1,2-insertion products (as shown in Table 1) from CH_2OO bimolecular reactions were calculated with the Nannoolal/Nannoolal method.[66] The partitioning coefficient is proportional to the aerosol/gas phase concentration ratio of species,[67] the magnitude of which indicates the extent of gas-aerosol partitioning. The partitioning coefficients (as shown in Table 2) were calculated according to the Pankow absorption model.[68,69] A larger value indicates a stronger tendency toward forming an aerosol. Table 2 shows that the product of the CH_2OO reaction with *tert*-butylamine has the third largest partitioning coefficient, only smaller than those with ammonia and water.

Some 1,2-insertion reactions that SCIs participate in can be significantly accelerated by the existence of water. For example, the reaction of *syn*-CH_3CHOO with NH_3 is more than 100 times faster at high humidity (water concentration of 10^{17} cm^{-3}) at 298 K and 250 Torr.[53] If the reaction of SCIs with *tert*-butylamine follows a similar trend, the atmospheric implications of this reaction should be considered, especially under high humidity conditions.

5. CONCLUSION

The bimolecular reaction rate coefficients of the simplest Criegee intermediate CH_2OO with *tert*-butylamine were measured with the OH laser-induced fluorescence method. The rate coefficient was measured to be $(4.95 \pm 0.64) \times 10^{-12}$ cm^3 $molecule^{-1}$ s^{-1} at 298 K. This reaction is observed to be negative temperature-dependent; the activation energy of (-2.82 ± 0.37) kcal mol^{-1} and the pre-exponential factor of $(4.21 \pm 0.55) \times 10^{-14}$ cm^3 $molecule^{-1}$ s^{-1} were derived from the Arrhenius equation. No obvious pressure dependence was observed at pressures from 5 to 75 Torr. Regarding the atmospheric effect, the adduction product—functionalized hydroperoxide of the title reaction might contribute to forming an organic aerosol.

https://doi.org/10.1021/acs.jpca.2c07854
J. Phys. Chem. A 2023, 127, 2432−2439

■ ASSOCIATED CONTENT

Supporting Information

The Supporting Information is available free of charge at https://pubs.acs.org/doi/10.1021/acs.jpca.2c07854.

Experimental conditions, error analysis, fitting parameters, energy profile of the reaction path, BDE and rate coefficients for different 1,2-insertion reactions (PDF)

■ AUTHOR INFORMATION

Corresponding Author

Wenrui Dong − *State Key Laboratory of Molecular Reaction Dynamics, Dalian Institute of Chemical Physics, Chinese Academy of Sciences, Dalian 116023, China;* orcid.org/0000-0002-3640-1821; Email: wrdong@dicp.ac.cn

Authors

Yang Chen − *Key Laboratory of Chemical Lasers, Dalian Institute of Chemical Physics, Chinese Academy of Sciences, Dalian 116023, China; University of Chinese Academy of Sciences, Beijing 100049, China; State Key Laboratory of Molecular Reaction Dynamics, Dalian Institute of Chemical Physics, Chinese Academy of Sciences, Dalian 116023, China*

Haotian Jiang − *State Key Laboratory of Molecular Reaction Dynamics, Dalian Institute of Chemical Physics, Chinese Academy of Sciences, Dalian 116023, China; Department of Chemical Physics, School of Chemistry and Materials Science, University of Science and Technology of China, Hefei 230026, China*

Siyue Liu − *State Key Laboratory of Molecular Reaction Dynamics, Dalian Institute of Chemical Physics, Chinese Academy of Sciences, Dalian 116023, China; Key Laboratory of Materials Modification by Laser, Ion, and Electron Beams, Chinese Ministry of Education, School of Physics, Dalian University of Technology, Dalian 116024, China*

Jiayu Shi − *State Key Laboratory of Molecular Reaction Dynamics, Dalian Institute of Chemical Physics, Chinese Academy of Sciences, Dalian 116023, China; Department of Physics, Dalian Maritime University, Dalian, Liaoning 116026, China*

Yuqi Jin − *University of Chinese Academy of Sciences, Beijing 100049, China; State Key Laboratory of Molecular Reaction Dynamics, Dalian Institute of Chemical Physics, Chinese Academy of Sciences, Dalian 116023, China*

Xueming Yang − *State Key Laboratory of Molecular Reaction Dynamics, Dalian Institute of Chemical Physics, Chinese Academy of Sciences, Dalian 116023, China; Department of Chemistry, Southern University of Science and Technology, Shenzhen 518055, China;* orcid.org/0000-0001-6684-9187

Complete contact information is available at: https://pubs.acs.org/10.1021/acs.jpca.2c07854

Notes

The authors declare no competing financial interest.

■ ACKNOWLEDGMENTS

The authors gratefully acknowledge the Dalian Coherent Light Source (DCLS) for support and assistance. This work was funded by the National Natural Science Foundation of China (NSFC No. 21873098, 22288201), Chinese Academy of Sciences (GJJSTD20220001), Liaoning Revitalization Talents Program (Grant No. XLYC1807248), and Innovation Program for Quantum Science and Technology (No. 2021ZD0303305).

■ REFERENCES

(1) Criegee, R. MECHANISM OF OZONOLYSIS. *Angew. Chem., Int. Ed. Engl.* **1975**, *14*, 745−752.

(2) Johnson, D.; Marston, G. The gas-phase ozonolysis of unsaturated volatile organic compounds in the troposphere. *Chem. Soc. Rev.* **2008**, *37*, 699−716.

(3) Pfeifle, M.; Ma, Y.-T.; Jasper, A. W.; Harding, L. B.; Hase, W. L.; Klippenstein, S. J. Nascent energy distribution of the Criegee intermediate CH_2OO from direct dynamics calculations of primary ozonide dissociation. *J. Chem. Phys.* **2018**, *148*, 174306.

(4) Novelli, A.; et al. Direct observation of OH formation from stabilised Criegee intermediates. *Phys. Chem. Chem. Phys.* **2014**, *16*, 19941−19951.

(5) Emmerson, K. M.; et al. Free radical modelling studies during the UK TORCH Campaign in Summer 2003. *Atmospheric Chemistry and Physics* **2007**, *7*, 167−181.

(6) Harrison, R. M.; et al. Measurement and modelling of air pollution and atmospheric chemistry in the UK West Midlands conurbation: Overview of the PUMA Consortium project. *Sci. Total Environ.* **2006**, *360*, 5−25.

(7) Elshorbany, Y. F.; et al. Oxidation capacity of the city air of Santiago, Chile. *Atmospheric Chemistry and Physics* **2009**, *9*, 2257−2273.

(8) Ren, X.; Brune, W. H.; Mao, J.; Mitchell, M. J.; Lesher, R. L.; Simpas, J. B.; Metcalf, A. R.; Schwab, J. J.; Cai, C.; Li, Y. Behavior of OH and HO_2 in the winter atmosphere in New York city. *Atmos. Environ.* **2006**, *40*, 252−263.

(9) Lu, Y.; Khalil, M.A.K. TROPOSPHERIC OH - MODEL-CALCULATIONS OF SPATIAL, TEMPORAL, AND SECULAR VARIATIONS. *Chemosphere* **1991**, *23*, 397−444.

(10) Holland, F.; Hofzumahaus, A.; Schafer, J.; Kraus, A.; Patz, H.-W. Measurements of OH and HO_2 radical concentrations and photolysis frequencies during BERLIOZ. *Journal of Geophysical Research-Atmospheres* **2003**, *108*, PHO 2-1.

(11) Khan, M. A. H.; et al. Criegee intermediates and their impacts on the troposphere. *Environmental Science-Processes & Impacts* **2018**, *20*, 437−453.

(12) Lewis, T. R.; et al. Direct evidence for a substantive reaction between the Criegee intermediate, CH_2OO, and the water vapour dimer. *Phys. Chem. Chem. Phys.* **2015**, *17*, 4859−4863.

(13) Chao, W.; et al. Direct kinetic measurement of the reaction of the simplest Criegee intermediate with water vapor. *Science* **2015**, *347*, 751−754.

(14) Luo, P. L.; Chung, C. A.; Lee, Y. P. Rate coefficient of the reaction $CH_2OO + NO_2$ probed with a quantum-cascade laser near 11 μm. *Phys. Chem. Chem. Phys.* **2019**, *21*, 17578−17583.

(15) Howes, N. U. M.; et al. Kinetic studies of C-1 and C-2 Criegee intermediates with SO_2 using laser flash photolysis coupled with photoionization mass spectrometry and time resolved UV absorption spectroscopy. *Phys. Chem. Chem. Phys.* **2018**, *20*, 22218−22227.

(16) Chao, W.; et al. Temperature and isotope effects in the reaction of CH_3CHOO with methanol. *Phys. Chem. Chem. Phys.* **2019**, *21*, 13633−13640.

(17) Chhantyal-Pun, R.; et al. Temperature-Dependence of the Rates of Reaction of Trifluoroacetic Acid with Criegee Intermediates. *Angew. Chem., Int. Ed.* **2017**, *56*, 9044−9047.

(18) Novelli, A.; et al. Estimating the atmospheric concentration of Criegee intermediates and their possible interference in a FAGE-LIF instrument. *Atmospheric Chemistry and Physics* **2017**, *17*, 7807−7826.

(19) Vereecken, L.; Novelli, A.; Taraborrelli, D. Unimolecular decay strongly limits the atmospheric impact of Criegee intermediates. *Phys. Chem. Chem. Phys.* **2017**, *19*, 31599−31612.

(20) Seinfeld, J. H. ES Books: Atmospheric Chemistry and Physics of Air Pollution. *Environ. Sci. Technol.* **1986**, *20*, 863.

(21) Ge, X. L.; Wexler, A. S.; Clegg, S. L. Atmospheric amines - Part I. A review. *Atmos. Environ.* **2011**, *45*, 524−546.

(22) Claeson, A. S.; Ostin, A.; Sunesson, A. L. Development of a LC-MS/MS method for the analysis of volatile primary and secondary amines as NIT (naphthylisothiocyanate) derivatives. *Anal. Bioanal. Chem.* **2004**, *378*, 932−939.
(23) Sorooshian, A.; et al. Comprehensive airborne characterization of aerosol from a major bovine source. *Atmospheric Chemistry and Physics* **2008**, *8*, 5489−5520.
(24) Edgerton, E. S.; et al. Ammonia and ammonium measurements from the southeastern United States. *Atmos. Environ.* **2007**, *41*, 3339−3351.
(25) Rumburg, B.; et al. Atmospheric flux of ammonia from sprinkler application of dairy waste. *Atmos. Environ.* **2006**, *40*, 7246−7258.
(26) Murphy, S. M.; et al. Secondary aerosol formation from atmospheric reactions of aliphatic amines. *Atmospheric Chemistry and Physics* **2007**, *7*, 2313−2337.
(27) Barsanti, K. C.; Pankow, J. F. Thermodynamics of the formation of atmospheric organic particulate matter by accretion reactions - Part 3: Carboxylic and dicarboxylic acids. *Atmos. Environ.* **2006**, *40*, 6676−6686.
(28) Chhantyal-Pun, R.; et al. Experimental and computational studies of Criegee intermediate reactions with NH_3 and CH_3NH_2. *Phys. Chem. Chem. Phys.* **2019**, *21*, 14042−14052.
(29) Chhantyal-Pun, R.; Khan, M. A. H.; Taatjes, C. A.; Percival, C. J.; Orr-Ewing, A. J.; Shallcross, D. E. Criegee intermediates: production, detection and reactivity. *Int. Rev. Phys. Chem.* **2020**, *39*, 385.
(30) Liu, Y. Q.; et al. A kinetic study of the CH_2OO Criegee intermediate reaction with SO_2, $(H_2O)_2$, CH_2I_2 and I atoms using OH laser induced fluorescence. *Phys. Chem. Chem. Phys.* **2017**, *19*, 20786−20794.
(31) Liu, Y. Q.; et al. Kinetics of the reaction of the simplest Criegee intermediate with ammonia: a combination of experiment and theory. *Phys. Chem. Chem. Phys.* **2018**, *20*, 29669−29676.
(32) Zhou, X. H.; et al. Unimolecular Reaction Rate Measurement of syn-CH_3CHOO. *J. Phys. Chem. Lett.* **2019**, *10*, 4817−4821.
(33) Atkinson, R.; et al. Evaluated kinetic and photochemical data for atmospheric chemistry: Volume IV - gas phase reactions of organic halogen species. *Atmospheric Chemistry and Physics* **2008**, *8*, 4141−4496.
(34) Eskola, A. J.; et al. Kinetics of the reactions of CH_2Br and CH_2I radicals with molecular oxygen at atmospheric temperatures. *Phys. Chem. Chem. Phys.* **2006**, *8*, 1416−1424.
(35) Stone, D.; et al. Unimolecular decomposition kinetics of the stabilised Criegee intermediates CH_2OO and CD_2OO. *Phys. Chem. Chem. Phys.* **2018**, *20*, 24940−24954.
(36) Peltola, J.; et al. Time-resolved, broadband UV-absorption spectrometry measurements of Criegee intermediate kinetics using a new photolytic precursor: unimolecular decomposition of CH_2OO and its reaction with formic acid. *Phys. Chem. Chem. Phys.* **2020**, *22*, 11797−11808.
(37) Huang, Y.-H.; Li, J.; Guo, H.; Lee, Y.-P. Infrared spectrum of the simplest Criegee intermediate CH_2OO at resolution 0.25 cm^{-1} and new assignments of bands 2 nu(9) and nu(5). *J. Chem. Phys.* **2015**, *142*, 214301.
(38) Nakajima, M.; et al. An experimental and theoretical study on rotational constants of vibrationally excited CH_2OO. *Chem. Phys. Lett.* **2015**, *621*, 129−133.
(39) Liu, Y. Q.; et al. Temperature- and pressure-dependent rate coefficient measurement for the reaction of CH_2OO with CH_3CH_2CHO. *Phys. Chem. Chem. Phys.* **2020**, *22*, 25869−25875.
(40) Lehman, J. H.; Li, H. W.; Lester, M. I. Ion imaging studies of the photodissociation dynamics of CH_2I_2 at 248 nm. *Chem. Phys. Lett.* **2013**, *590*, 16−21.
(41) Berndt, T.; et al. Kinetics of the unimolecular reaction of CH_2OO and the bimolecular reactions with the water monomer, acetaldehyde and acetone under atmospheric conditions. *Phys. Chem. Chem. Phys.* **2015**, *17*, 19862−19873.
(42) Liu, S. Y.; et al. Experimental and Computational Studies of Criegee Intermediate syn-CH3CHOO Reaction with Hydrogen Chloride. *J. Phys. Chem. A* **2021**, *125*, 8587−8594.
(43) Zhou, X.; Chen, Y.; Liu, Y.; Li, X.; Dong, W.; Yang, X. Kinetics of CH_2OO and syn-CH_3CHOO reaction with acrolein. *Phys. Chem. Chem. Phys.* **2021**, *23*, 13276.
(44) Mir, Z. S.; et al. CH_2OO Criegee intermediate UV absorption cross-sections and kinetics of CH_2OO + CH_2OO and CH_2OO + I as a function of pressure. *Phys. Chem. Chem. Phys.* **2020**, *22*, 9448−9459.
(45) McGillen, M. R.; et al. Criegee Intermediate-Alcohol Reactions, A Potential Source of Functionalized Hydroperoxides in the Atmosphere. *Acs Earth and Space Chemistry* **2017**, *1*, 664−672.
(46) Chao, W.; et al. Effects of water vapor on the reaction of CH_2OO with NH_3. *Phys. Chem. Chem. Phys.* **2019**, *21*, 22589−22597.
(47) *CRC Handbook of Chemistry and Physics*, 96th ed.; Haynes, W. M., Ed.; CRC Press, 2016; p 423.
(48) Lin, L. C.; et al. Competition between H_2O and $(H_2O)_2$ reactions with CH_2OO/CH_3CHOO. *Phys. Chem. Chem. Phys.* **2016**, *18*, 4557−4568.
(49) Sheps, L.; et al. The reaction of Criegee intermediate CH_2OO with water dimer: primary products and atmospheric impact. *Phys. Chem. Chem. Phys.* **2017**, *19*, 21970−21979.
(50) Sheps, L.; Scully, A. M.; Au, K. UV absorption probing of the conformer-dependent reactivity of a Criegee intermediate CH_3CHOO. *Phys. Chem. Chem. Phys.* **2014**, *16*, 26701−26706.
(51) Taatjes, C. A.; et al. Direct Measurements of Conformer-Dependent Reactivity of the Criegee Intermediate CH_3CHOO. *Science* **2013**, *340*, 177−180.
(52) Misiewicz, J. P.; et al. Re-examining ammonia addition to the Criegee intermediate: converging to chemical accuracy. *Phys. Chem. Chem. Phys.* **2018**, *20*, 7479−7491.
(53) Chao, W.; et al. Synergy of Water and Ammonia Hydrogen Bonding in a Gas-Phase Reaction Published as part of The Journal of Physical Chemistry virtual special issue "Hanna Reisler Festschrift". *J. Phys. Chem. A* **2019**, *123*, 1337−1342.
(54) Hubin-Franskin, M. J.; et al. Electronic excitation and optical cross sections of methylamine and ethylamine in the UV-VUV spectral region. *J. Chem. Phys.* **2002**, *116*, 9261−9268.
(55) Tan, W.; et al. Theoretical and Experimental Study on the Reaction of tert-Butylamine with OH Radicals in the Atmosphere. *J. Phys. Chem. A* **2018**, *122*, 4470−4480.
(56) Long, B.; Bao, J. L.; Truhlar, D. G. Atmospheric Chemistry of Criegee Intermediates: Unimolecular Reactions and Reactions with Water. *J. Am. Chem. Soc.* **2016**, *138*, 14409−14422.
(57) Li, Y. L.; Kuo, M. T.; Lin, J. M. Unimolecular decomposition rates of a methyl-substituted Criegee intermediate syn-CH_3CHOO. *Rsc Advances* **2020**, *10*, 8518−8524.
(58) Robinson, C.; Onel, L.; Newman, J.; Lade, R.; Au, K.; Sheps, L.; Heard, D. E.; Seakins, P. W.; Blitz, M. A.; Stone, D. Unimolecular Kinetics of Stabilized CH_3CHOO Criegee Intermediates: syn-CH_3CHOO Decomposition and anti-CH_3CHOO Isomerization. *J. Phys. Chem. A* **2022**, *126*, 6984.
(59) Kumar, M.; Francisco, J. S. Heteroatom Tuning of Bimolecular Criegee Reactions and Its Implications. *Angew. Chem., Int. Ed.* **2016**, *55*, 13432−13435.
(60) Smith, M. C.; et al. Temperature-Dependent Rate Coefficients for the Reaction of CH_2OO with Hydrogen Sulfide. *J. Phys. Chem. A* **2017**, *121*, 938−945.
(61) Tadayon, S. V.; Foreman, E. S.; Murray, C. Kinetics of the Reactions between the Criegee Intermediate CH_2OO and Alcohols. *J. Phys. Chem. A* **2018**, *122*, 258−268.
(62) Cabezas, C.; Endo, Y. Probing Criegee intermediate reactions with methanol by FTMW spectroscopy. *Phys. Chem. Chem. Phys.* **2020**, *22*, 13756−13763.
(63) Aroeira, G. J. R.; et al. The addition of methanol to Criegee intermediates. *Phys. Chem. Chem. Phys.* **2019**, *21*, 17760−17771.
(64) Riipinen, I.; et al. Adipic and malonic acid aqueous solutions: Surface tensions and saturation vapor pressures. *J. Phys. Chem. A* **2007**, *111*, 12995−13002.

https://doi.org/10.1021/acs.jpca.2c07854
J. Phys. Chem. A 2023, 127, 2432−2439

(65) Koponen, I. K.; et al. Thermodynamic properties of malonic, succinic, and glutaric acids: Evaporation rates and saturation vapor pressures. *Environ. Sci. Technol.* **2007**, *41*, 3926−3933.
(66) Nannoolal, Y.; Rarey, J.; Ramjugernath, D. Estimation of pure component properties - Part 3. Estimation of the vapor pressure of non-electrolyte organic compounds via group contributions and group interactions. *Fluid Phase Equilib.* **2008**, *269*, 117−133.
(67) Odum, J. R.; et al. Gas/particle partitioning and secondary organic aerosol yields. *Environ. Sci. Technol.* **1996**, *30*, 2580−2585.
(68) Pankow, J. F. AN ABSORPTION-MODEL OF THE GAS AEROSOL PARTITIONING INVOLVED IN THE FORMATION OF SECONDARY ORGANIC AEROSOL. *Atmos. Environ.* **1994**, *28*, 189−193.
(69) Jenkin, M. E. Modelling the formation and composition of secondary organic aerosol from alpha- and beta-pinene ozonolysis using MCM v3. *Atmospheric Chemistry and Physics* **2004**, *4*, 1741−1757.

https://doi.org/10.1021/acs.jpca.2c07854
J. Phys. Chem. A 2023, 127, 2432−2439